# Comparison of Radiative Transfer Models for Simulating Snow Surface Thermal Infrared Emissivity

Jie Cheng, Shunlin Liang, *Senior Member, IEEE*, Fuzhong Weng, Jindi Wang, and Xiaowen Li

***Abstract*—In this study, three analytical radiative transfer (RT) models and a numerical RT model are used to simulate the thermal-infrared (8-13 $\mu$m) emissivity spectra of snow surfaces. The single-scattering albedo and asymmetry factor calculated by Mie theory, in conjunction with that modified by two existing packing correction methods, are used as inputs to these RT models. The simulated snow emissivity spectra are compared with *in situ* measurements. The best models for simulating snow emissivity spectra are identified at the conclusion of this paper.**

***Index Terms*—DISORT, Mie theory, radiative transfer model, snow emissivity spectra.**

## I. Introduction

SNOW cover has a strong impact on surface energy balance. Snow spectral emissivity is a key parameter for the accurate determination of snow surface temperature, which is an indicator of cryospheric climate change and often used as an initial value in climate models [1], [2]. This parameter also determines the long-wave upwelling radiation of snow surfaces. Moreover, remote sensing of atmospheric temperature-humidity profiles and trace gases over snow surfaces, using a nadir-view sensor, requires *a priori* snow emissivity for accurate retrieval [3]–[5].

However, snow spectral emissivity is treated roughly and often assigned as a constant in current climate models. For example, operational algorithms for processing Geostationary Operational Environmental Satellite (GOES) data use a gray-body emissivity of 0.96 for land surfaces [3]; the ECMWF model sets a constant for all land surfaces for their monitoring purposes [6]; and the NCAR Community Land Model Version 2 (CLM2) calculates canopy emissivity from LAI, and sets soil and snow emissivities as 0.96 and 0.97 [7]. The spectral and view-angle dependence of snow emissivity are omitted completely in these studies. A model with a strong physical foundation, capable of modeling snow emissivity spectra for climate studies, is urgently needed.

This paper examines several radiative transfer (RT) models and compares the simulated snow directional emissivity with ground measurements in the field. Section II introduces the radiative transfer models. Section III describes the complex refraction index of snow particles, field measured snow parameters, and the simulated single-scattering properties. The comparison results are presented in Section IV. A brief conclusion and discussion is provided in Section V.

Manuscript received July 24, 2009; revised December 22, 2009; accepted May 07, 2010. Date of publication July 08, 2010; date of current version August 25, 2010. This work was supported in part by the Special Fund for Young Talents of the State Key Laboratory of Remote Sensing Sciences under Grant 270401GK, the National Oceanic Atmospheric Administration under Grant NA07NES4400001, the National High Technology Research and Development Program of China under Grant 2009AA122100, the National Basic Research Program of China under Grants 2007CB714400 and 2007CB714407, and by the National Natural Science Foundation of China under Grant 40901167.

J. Cheng is with the State Key Laboratory of Remote Sensing Sciences, Jointly Sponsored by Beijing Normal University and Chinese Academy of Sciences, Beijing 100875, China, and also with the College of Global Change and Earth System Science, Beijing Normal University, Beijing 100875, China, and the Department of Geography, University of Maryland, College Park, MD 20742 USA (e-mail: brucechan2003@126.com).

J. Wang and X. Li are with the State Key Laboratory of Remote Sensing Sciences, Jointly Sponsored by Beijing Normal University and Chinese Academy of Sciences, Beijing 100875, China.

S. Liang is with the Department of Geography, University of Maryland, College Park, MD 20742 USA.

F. Weng is with the NOAA/NESDIS/Center for Satellite Applications and Research, Camp Springs, MD 20746 USA.

Digital Object Identifier 10.1109/JSTARS.2010.2050300

## II. Radiative Transfer Models

### A. Mie Single-Scattering Theory

When a plane electromagnetic wave is incident upon a uniform spherical scattering particle, its power will be redistributed and it will propagate along different directions. The relocation of the incident power along different directions depends on the size parameter and the complex refractive index of the particle. Mie gives a mathematically rigorous solution for scattering by uniform spherical particles, and the solution is known as the Mie theory [8]. In the Mie theory, all types of photo-particle interactions such as reflection, refraction and diffraction are included. Given the size parameter $x = 2\pi r/\lambda$, where $r$ is the sphere radius and $\lambda$ is the wavelength of incident wave; and complex refractive index $m = n + ik$, where $n$ is the real part and $k$ is the imaginary part; the Mie theory can calculate the single-scattering albedo $\omega$ and the scattering phase function $P(\theta)$, where $\theta$ is the scattering angle. $\omega$ represents the ratio of total scattering light to incident light, and $P(\theta)$ represents the probability that the light scatters into the scattering angle $\theta$. The asymmetry parameter $g = (1/2)\int_{-1}^{1} P(\theta)\cos\theta d(\cos\theta)$ is the integrated value of phase function weighted with the cosine of the scattering angle $\theta$. Together, single-scattering parameters (e.g., $\omega$ and $g$) determine the behavior of a photon in the statistical sense, and provide the basis of the multiple-scattering calculation for a semi-infinite medium composed of many scattering particles.

### B. Mie/Conel Model

The Mie theory is a single-scattering theory and cannot be used to describe how light interacts with a plane surface composed of many scatter events in which multiple-scattering dominates. Conel developed a cloudy atmosphere model of powder emission spectrums in which the Mie theory is used to calculate single-scattering parameters, and where multiple-scattering is modeled with a two-stream approximation [9]. This model is hereafter referred to as the Mie/Conel model. Surface emissivity is simulated as

$$\varepsilon = \frac{2}{u+1} \tag{1}$$

where $u^2 = (1-\omega g/3)(1-\omega)^{-1}$. The directionality of emissivity is not considered in the Mie/Conel model as we can see from (1). This model is also invalid for isotropic and conservative scattering when $g = 0$ and $\omega = 1$.

Although an independent scattering approximation is a poor assumption for a semi-infinite medium, where scattering particles are touched together and always closely packed, the accuracy of the Mie/Conel model is justified by their laboratory experiments [9].

### C. Mie/DW Model

Based on the snow spectral albedo model developed by Wiscombe and Warren [10], Dozier and Warren derived a formulation for snow directional emissivity spectra modeling [11]. In their model, the Mie theory is used for single-scattering, and the $\delta$-Eddington approximation [12] is used for multiple-scattering. This model is referred to as the Mie/DW model:

$$\varepsilon_s(\lambda, \mu_v) = \frac{\xi\mu_v[\omega^* b^* + 1 + P] + 1 + P + \omega^*}{(1+P)(1+\xi\mu_v)} \tag{2}$$

where $\varepsilon_s(\lambda, \mu_v)$ is the directional emissivity at wavelength $\lambda$ and viewing angle $\mu_v$. $\mu_v = \cos\theta_v$, $\theta_v$ is the zenith angle of surface-emitted radiation. The other variables in (2) are given as

$$\begin{aligned} g^* &= \frac{g}{1+g} \\ \omega^* &= \frac{(1-g^2)\omega}{1-g^2\omega} \\ b^* &= \frac{g^*}{1-\omega^* g^*} \\ \xi &= [3(1-\omega^* g^*)(1-\omega^*)]^{1/2} \\ P &= \frac{2\xi}{3(1-\omega^* g^*)} \end{aligned}$$

where $g^*$ and $\omega^*$ are the delta-Eddington transformations of $g$ and $\omega$ [12]. $b^*$, $\xi$, and $P$ are middle variables.

### D. Mie/Hapke Model

Since 1981, Hapke has developed several analytical bidirectional reflectance models for planetary studies [13]–[16]. Some of these have been revised for soils and vegetation [17], [18]. Proposed in 1993 [16], Hapke's emission theory is used to model snow directional emissivity spectra in this study. When the Mie theory is used for single-scattering, we refer to it as the Mie/Hapke model. Surface directional emissivity spectra is denoted as

$$\varepsilon_d(e) = \gamma H(\mu) \tag{3}$$

where $\gamma = (1-w)^{1/2}$ and $H(\mu)$ is Chandrasekhar's H function, which can be approximated by $H(x) = (1+2x)/(1+2\gamma x)$.

### E. Mie/DISORT Model

DISORT is a well-tested and validated numerical multiple-scattering radiative transfer model, and is often used as a metric to evaluate the performance of other models [19], [20]. DISORT is used to calculate the hemispherical directional reflectance of snow surfaces, in which the Mie theory is used for single-scattering. Surface emissivity is derived via Kirchhoff's law. This combination is referred to as the Mie/DISORT model.

### F. Mie Corrections

Independent scattering is an accepted assumption for atmospheric radiative transfer problems where scattering media are far apart in comparison to their size. However, it is a poor assumption for a semi-infinite medium in which scattering particles are touching and at times densely packed. As demonstrated by Hulst [21], the distances between neighboring particles must be at least three particle radii for the independent scattering approximation to be valid. In actuality, the snow medium does not meet this requirement. Consequently, direct use of the Mie parameters in multiple-scattering may not be appropriate. Two methods were proposed to correct the Mie parameters to consider the packing conditions in a semi-infinite medium. One is the diffraction subtraction method proposed by Wald [22], [23]. The other is the static structure factor correction proposed by Mishchenko [24], [25].

In a closely packed semi-infinite medium, forward scattered light can not be distinguished from unscattered light. For larger particles, the reflected, refracted and diffracted components of scattered light can be treated independently. Based on the assumption that the diffraction scattering efficiency is unity and the asymmetry factor of diffracted light is one, Wald derived the formulation for diffraction subtraction:

$$\begin{cases} w_d = 2w_m - 1 \\ g_d = \frac{(2w_m g_m - 1)}{(2w_m - 1)} \end{cases} \tag{4}$$

where $w_d$ and $g_d$ are the corrected single-scattering albedo and asymmetry factor. $w_m$ and $g_m$ are the Mie parameters, including diffraction.

Static structure factor correction has a strong physical foundation and is based on solving Maxwell's equation for light scattering and on statistical mechanics for dense packing. The Mie parameters are modified via a static structure factor $S(\theta)$, which is given by

$$S(\theta) = \frac{1}{1 - n_d C(p)} \tag{5}$$

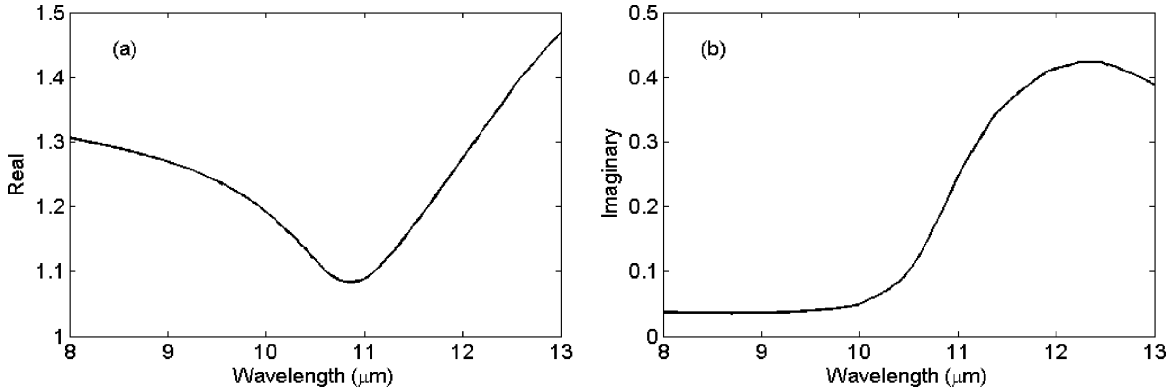


Fig. 1. Complex refractive index of ice in thermal infrared: (a) real part; (b) imaginary part.

TABLE I
SNOW PARTICLE SIZE MEASURED DURING THE FIELD MEASUREMENTS. TYPES 1–4 REPRESENT FINE DENDRITE SNOW, MEDIUM GRAIN SNOW, COARSE GRANULAR SNOW, AND SUN CRUST, RESPECTIVELY

| Snow type | Type 1 | Type 2 | Type 3 | Type 4 |
|---|---|---|---|---|
| Min-diameter (μm) | 40 | 300 | 50 | 800 |
| Median-diameter (μm) | 70 | 600 | 800 | 1100 |
| Max-diameter (μm) | 100 | 1100 | 1000 | 1500 |

where

$$C(p) = 24\frac{f}{n_d}\left[\frac{\alpha+\beta+\delta}{u^2}\cos u - \frac{\alpha+2\beta+4\delta}{u^3}\sin u - \frac{2(\beta+6\delta)}{u^4}\cos u + \frac{2\beta}{u^4} + \frac{24\delta}{u^5}\sin u + \frac{24\delta}{u^6}(\cos u - 1)\right], \quad p \neq 0.$$

For the special case of $p = 0$, $C(0) = -24(f/n)(\alpha/3 + \beta/4 + \delta/6)$. $p = (4\pi\sin(\theta/2))/\lambda$, $\lambda$ is the wavelength of incident light. $n_d$ is the number density of scattering particles. $f = (4\pi n_d r^3)/3$ is the filling factor, i.e., the ratio of a volume of spheres to the volume of the smallest cube that can enclose them. $r$ is the particle radius. Other parameters are defined as

$$u = 2pr$$
$$\alpha = \frac{(1+2f)^2}{(1-f)^4}$$
$$\beta = -6f\frac{\left(1+\frac{f}{2}\right)^2}{(1-f)^4}$$
$$\delta = \frac{\alpha f}{2}.$$

The modified Mie parameters are given as

$$\begin{cases} \omega_{ssfc}(f) = \dfrac{(1+\omega^{RT})B(f)}{(1+\omega^{RT})B(f) - \omega^{RT} + 1} \\ g_{ssfc} = \dfrac{\int_{-1}^{1}[p(\theta)S(\theta)]\cos\theta d(\cos\theta)}{\int_{-1}^{1}[p(\theta)S(\theta)]d(\cos\theta)} \end{cases} \quad (6)$$

where $B(f) = (1/2)\int_{-1}^{1}[p(\theta)S(\theta)]d(\cos\theta)$ is the ratio of the scattering cross section of densely packed particles to that of isolated particles. $\omega^{RT}$ is the ray-tracing single-scattering albedo.

### G. Mie-Corrected Models

The Mie parameters modified by two correction methods are used as inputs to the previous models, and the resulted models are referred as the Mie-Wald/Conel model and the Mie-Mishchenko/Conel model, the Mie-Wald/Hapke model and the Mie-Mishchenko/Hapke model, the Mie-Wald/DISORT model and the Mie-Mishchenko/DISORT model, respectively.

## III. DATA

### A. Complex Refractive Index

The complex refractive index is one of the two key parameters used by the Mie theory for the calculation of single-scattering parameters. Warren compiled a complex refractive index of ice that is used for this study and is shown in Fig. 1 [26], [27].

### B. Snow Parameters

M. Hori at EORC/JAEA conducted field measurements of snow directional emissivity spectra from February 2002 to March 2004, using a portable Fourier transform infrared spectrometer, while conducting snow pit work [28]. His data is used in this work. The snow particle size is presented in Table I. Measured snow directional emissivity spectra are shown in Fig. 2.

### C. Simulated Mie Parameters

Given the complex refractive index, particle size distribution and wavelength, the Mie code provided by W. Wiscombe at NASA/GSFC [29] is used to calculate the Mie parameters. Although realistic snow particles are non-spherical, equivalent

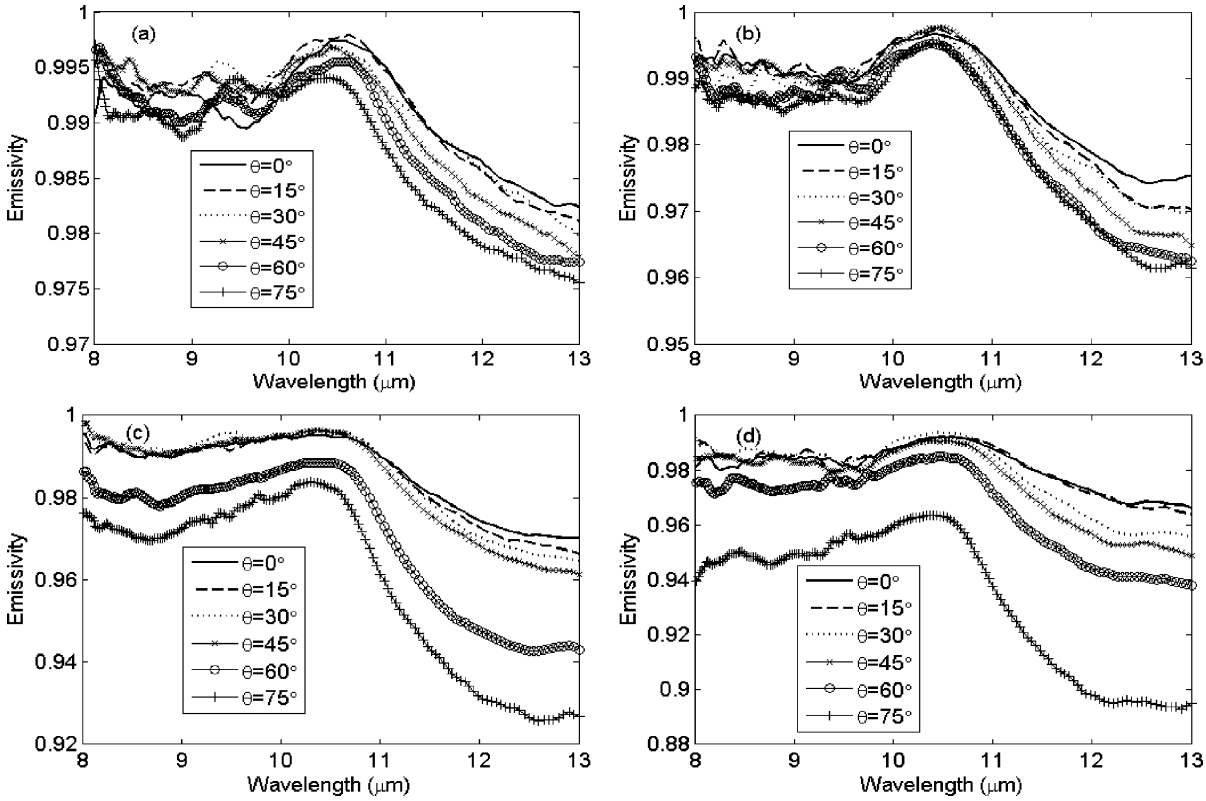


Fig. 2. Field measurements of snow directional emissivity spectra: (a) fine dendrite snow; (b) medium grain snow; (c) coarse granular snow; (d) sun crust.

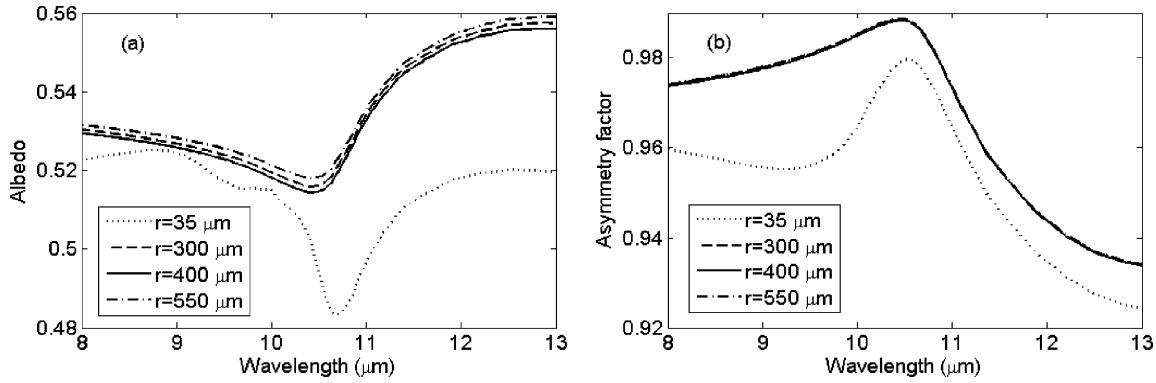


Fig. 3. Mie parameters of the indicated radius as calculated by Mie theory: (a) single-scattering albdo; (b) asymmetry factor.

spheres are commonly used to represent and simplify snow grains [10], [30]–[34]. Mean snow particle radii is specified as that of equivalent spheres in this work. The distribution of snow particles is described using log normal distribution. Its expression is given by [35]

$$n(r) = (const) \times r^{-1} \exp\left(-\frac{(\ln r - \ln r_g)^2}{2\ln^2 \sigma_g}\right) \qquad (7)$$

where $r_g$ is the effective radius and $\sigma_g$ is the standard deviation of radius. The calculated Mie parameters are shown in Fig. 3.

### D. Corrected Mie Parameters

The corrected Mie parameters are shown in Figs. 4 and 5. The lower radius size limit on the applicability of diffraction subtraction is 50 $\mu$m [22], and the Mie parameters for three radii are shown in Fig. 4. Mie parameters corrected by the static structure factor are calculated for f = 0.1, 0.2, 0.3, 0.4, 0.5, and 0.6. Their difference is not pronounced, and only that for f = 0.2 is shown in Fig. 5. (It can be considered densely packed when f $\geq$ 0.05.)

## IV. Results

### A. Mie/Conel Model

The simulated and field-measured snow nadir emissivity spectra are shown in Fig. 6. The shape of snow emissivity spectrum is effectively simulated. The simulated snow emissivity is lower than the measured snow emissivity. The spectral variability of simulated emissivity spectra between different snow particle radii is not significant, specifically in the 8-10.5 $\mu$m spectral region. The simulated emissivity spectra are almost

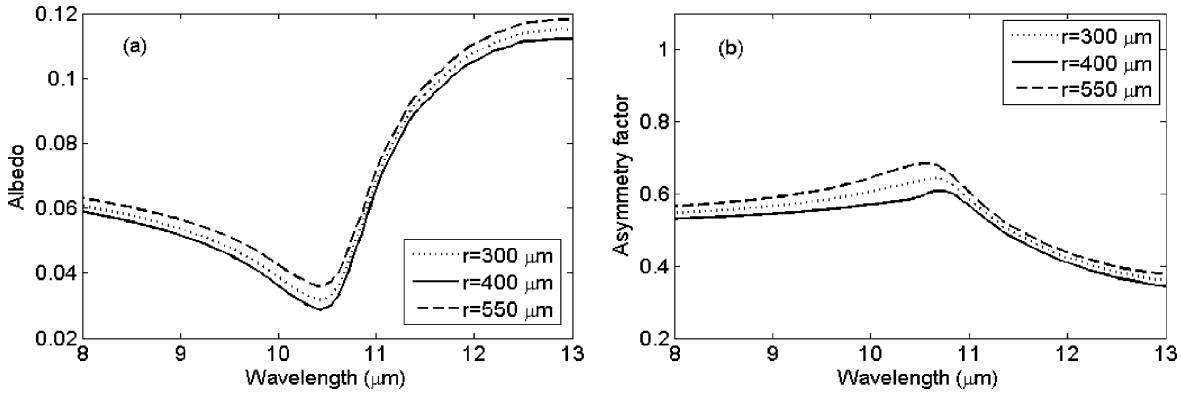


Fig. 4. Mie parameters of the indicated radius, as calculated by Mie theory, and corrected by Wald's method: (a) single-scattering albedo; (b) asymmetry factor.

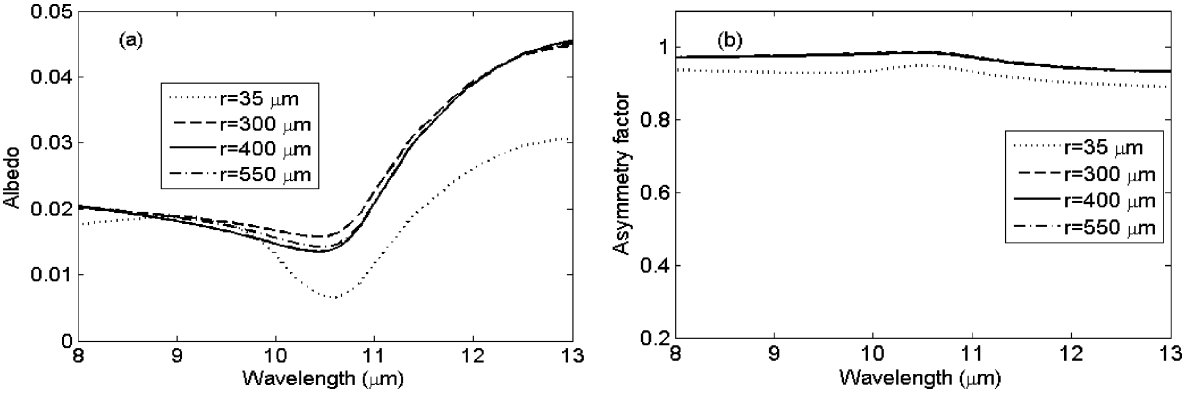


Fig. 5. Mie parameters of the indicated radius, as calculated by Mie theory, and corrected by Mishenko's method: (a) single-scattering albedo; (b) asymmetry factor. f = 0.2.

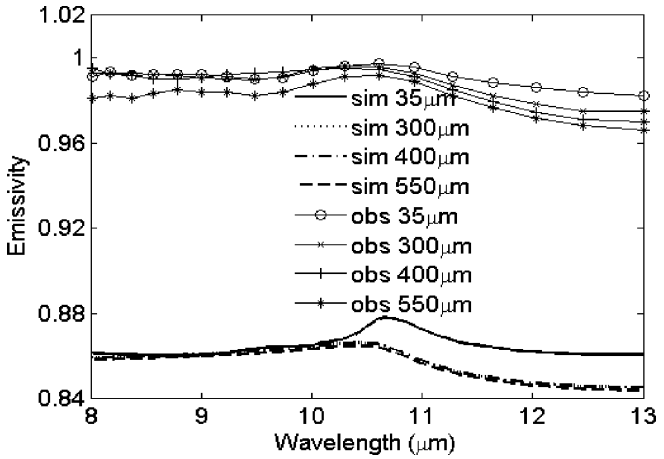


Fig. 6. Comparison of field measured snow nadir emissivity spectra with that simulated by the Mie/Conel model. For clarification, the measured emissivity spectra are averaged every nine wavelength points.

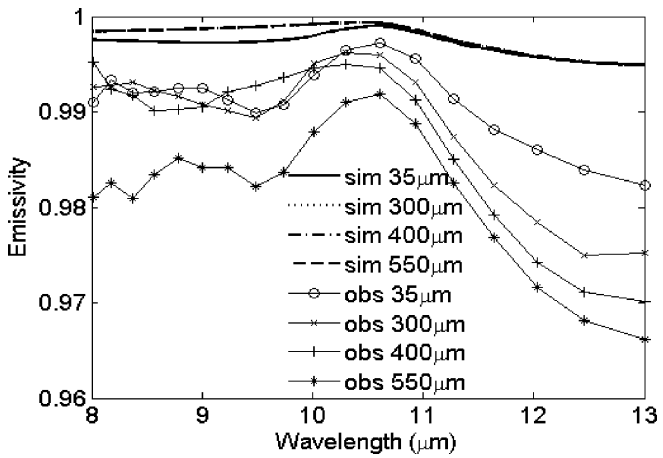


Fig. 7. Comparison of field-measured snow nadir emissivity spectra with that simulated by the Mie/DW model.

unchanged for larger particles. The increase in snow particle size due to packing or welding will increase surface scattering and the reappearance of reststrahlen bands. The emissivity will decrease with increasing particle size according to the Kirchhoff's Law. The radial dependence of snow emissivity, such as the decrease in snow emissivity with an increasing particle radius, is reflected in the measured data. As shown in Table II, the root mean square error (RMSE) of simulated emissivity is very large and lies between 0.123 and 0.131 in the 8-11 $\mu$m and 11-13 $\mu$m spectral regions. This implies that the Mie/Conel model is not appropriate for snow surface emissivity modeling.

### *B. Mie/DW Model*

The simulated and field-measured snow nadir emissivity spectra are shown in Fig. 7. The shape of the snow emissivity spectrum is well simulated. The simulated snow emissivity is

TABLE II
RMSE OF SIMULATED NADIR EMISSIVITIES USING DIFFERENT RT MODELS IN THE 8-11 $\mu$m AND 11-13 $\mu$m SPECTRAL REGIONS. "—" DENOTES THAT WALD'S METHOD DOES NOT WORK

| RT models | RMSE | | | | | | | |
|---|---|---|---|---|---|---|---|---|
| | 8-11 μm | | | | 11-13 μm | | | |
| | Type 1 | Type 2 | Type 3 | Type 4 | Type 1 | Type 2 | Type 3 | Type 4 |
| Mie/Conel | 0.128 | 0.130 | 0.130 | 0.124 | 0.123 | 0.131 | 0.128 | 0.126 |
| Mie/DW | 0.005 | 0.007 | 0.006 | 0.014 | 0.009 | 0.016 | 0.020 | 0.023 |
| Mie/Hapke | 0.120 | 0.123 | 0.123 | 0.117 | 0.114 | 0.121 | 0.117 | 0.116 |
| Mie/DISORT | 0.201 | 0.206 | 0.205 | 0.198 | 0.195 | 0.209 | 0.205 | 0.204 |
| Mie-Wald/Conel | - | 0.004 | 0.003 | 0.005 | - | 0.004 | 0.003 | 0.003 |
| Mie-Mishchenko/Conel | 0.005 | 0.005 | 0.005 | 0.012 | 0.009 | 0.014 | 0.017 | 0.020 |
| Mie-Wald/Hapke | - | 0.002 | 0.001 | 0.006 | - | 0.003 | 0.007 | 0.008 |
| Mie-Mishchenko/Hapke | 0.005 | 0.005 | 0.005 | 0.012 | 0.009 | 0.014 | 0.018 | 0.020 |
| Mie-Wald/DISORT | - | 0.008 | 0.007 | 0.003 | - | 0.012 | 0.008 | 0.007 |
| Mie-Mishchenko/DISORT | 0.003 | 0.003 | 0.003 | 0.010 | 0.006 | 0.009 | 0.013 | 0.015 |

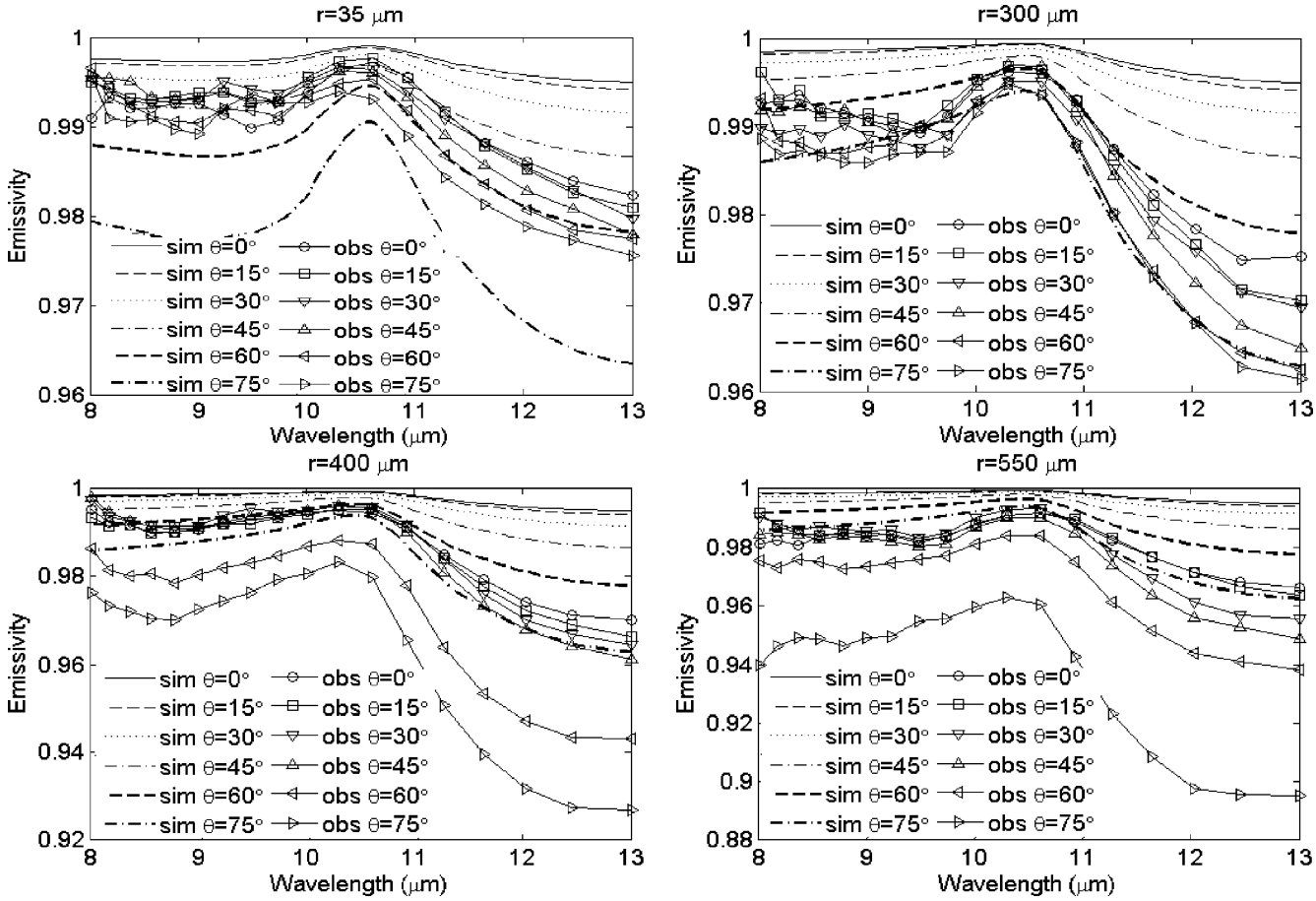


Fig. 8. Comparison of field-measured snow directional emissivity spectra with that simulated by the Mie/DW model.

larger than the measured snow emissivity. The spectral variability of simulated emissivity spectra between different snow particle radii is not pronounced, especially in the 11-13 $\mu$m spectral region. The simulated emissivity spectra are almost unchanged for larger particles. The radial dependence of snow emissivity is not reflected in the simulated data. Furthermore, snow emissivity for large particles is higher than that for small particles within the 8-12 $\mu$m spectral region. The RMSE of simulated emissivity in 8-11 $\mu$m is lower than that in 11-13 $\mu$m. In the former spectral region, the RMSE are 0.005, 0.007, 0.006, and 0.014, for r = 35, 300, 400, and 550 $\mu$m, respectively (Table II).

Fig. 8 shows the simulated directional emissivity spectra using the Mie/DW model. The shape of snow emissivity and the angular dependence, such as the decrease in snow emissivity with an increasing view angle, are well simulated. The simulated snow emissivity is larger than the measured snow emissivity, except for r = 35 $\mu$m. Table III shows the RMSE of simulated directional emissivity. The RMSE in the 8-11 $\mu$m spectral region is clearly lower than that in the 11-13 $\mu$m

TABLE III
RMSE OF SIMULATED DIRECTIONAL EMISSIVITY USING MIE/DW MODEL IN THE 8-11 $\mu$m AND 11-13 $\mu$m SPECTRAL REGIONS

| Observation angle | RMSE | | | | | | | |
|---|---|---|---|---|---|---|---|---|
| | 8-11 μm | | | | 11-13 μm | | | |
| | Type 1 | Type 2 | Type 3 | Type 4 | Type 1 | Type 2 | Type 3 | Type 4 |
| 0° | 0.005 | 0.007 | 0.006 | 0.014 | 0.009 | 0.016 | 0.020 | 0.023 |
| 15° | 0.003 | 0.006 | 0.006 | 0.013 | 0.010 | 0.018 | 0.020 | 0.023 |
| 30° | 0.002 | 0.008 | 0.004 | 0.011 | 0.008 | 0.017 | 0.021 | 0.029 |
| 45° | 0.002 | 0.004 | 0.003 | 0.012 | 0.006 | 0.016 | 0.019 | 0.030 |
| 60° | 0.004 | 0.004 | 0.011 | 0.017 | 0.001 | 0.012 | 0.031 | 0.034 |
| 75° | 0.012 | 0.002 | 0.014 | 0.038 | 0.010 | 0.013 | 0,034 | 0.065 |

TABLE IV
RMSE OF SIMULATED DIRECTIONAL EMISSIVITY USING MIE/HAPKE MODEL IN 8-11 $\mu$m AND 11-13 $\mu$m SPECTRAL REGIONS

| Observation angle | RMSE | | | | | | | |
|---|---|---|---|---|---|---|---|---|
| | 8-11 μm | | | | 11-13 μm | | | |
| | Type 1 | Type 2 | Type 3 | Type 4 | Type 1 | Type 2 | Type 3 | Type 4 |
| 0° | 0.120 | 0.123 | 0.123 | 0.117 | 0.114 | 0.121 | 0.117 | 0.116 |
| 15° | 0.124 | 0.126 | 0.125 | 0.121 | 0.116 | 0.122 | 0.119 | 0.118 |
| 30° | 0.132 | 0.132 | 0.135 | 0.130 | 0.124 | 0.130 | 0.126 | 0.119 |
| 45° | 0.148 | 0.150 | 0.150 | 0.143 | 0.137 | 0.144 | 0.140 | 0.131 |
| 60° | 0.172 | 0.174 | 0.166 | 0.162 | 0.161 | 0.169 | 0.149 | 0.147 |
| 75° | 0.215 | 0.218 | 0.204 | 0.182 | 0.203 | 0.215 | 0.181 | 0.152 |

TABLE V
RMSE OF SIMULATED DIRECTIONAL EMISSIVITY USING MIE/DISORT MODEL IN THE8-11 $\mu$m AND11-13 $\mu$m SPECTRAL REGIONS

| Observation angle | RMSE | | | | | | | |
|---|---|---|---|---|---|---|---|---|
| | 8-11 μm | | | | 11-13 μm | | | |
| | Type 1 | Type 2 | Type 3 | Type 4 | Type 1 | Type 2 | Type 3 | Type 4 |
| 0° | 0.201 | 0.206 | 0.205 | 0.198 | 0.195 | 0.209 | 0.205 | 0.204 |
| 15° | 0.162 | 0.165 | 0.164 | 0.159 | 0.154 | 0.163 | 0.160 | 0.160 |
| 30° | 0.139 | 0.139 | 0.142 | 0.137 | 0.130 | 0.137 | 0.133 | 0.127 |
| 45° | 0.125 | 0.127 | 0.127 | 0.120 | 0.114 | 0.120 | 0.116 | 0.107 |
| 60° | 0.116 | 0.117 | 0.109 | 0.104 | 0.105 | 0.108 | 0.089 | 0.087 |
| 75° | 0.113 | 0.113 | 0.099 | 0.077 | 0.101 | 0.105 | 0.072 | 0.042 |

spectral region. In the 8-11 $\mu$m spectral region, the RMSE for r = 35, 300, and 400 $\mu$m is less than 0.008, when the view zenith angle is less than 60 degrees. The RMSE for r = 550 $\mu$m is less than 0.014, on the condition that the view angle is less than 60 degrees.

### C. Mie/Hapke Model

The simulated nadir and directional snow emissivity spectra are shown in Figs. 9 and 10. The RMSE of simulated emissivity are very large, and lie between 0.114 and 0.218 in the 8-11 $\mu$m and 11-13 $\mu$m spectral regions (Tables II and IV). Similar to the Mie/Conel model, the Mie/Hapke model is not appropriate for snow surface emissivity modeling. The shape of snow emissivity, and its radial and angular dependence, is well simulated. The simulated snow emissivity is lower than the measured snow emissivity. The spectral variability of simulated snow emissivity between different view angles is larger than that of measured snow emissivity.

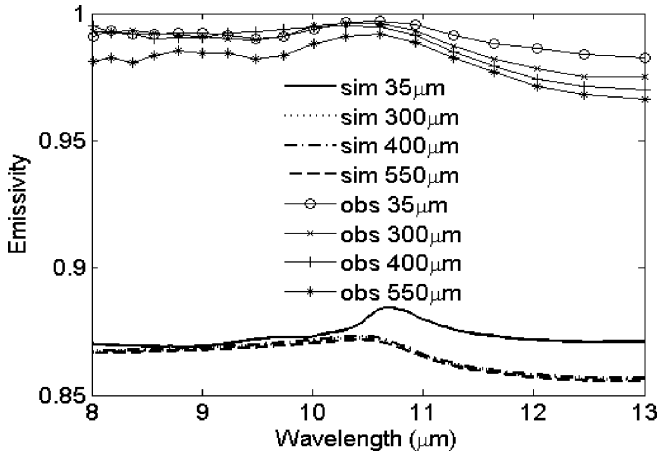


Fig. 9. Comparison of field-measured snow nadir emissivity spectra with that simulated by the Mie/Hapke model.

### D. Mie/DISORT Model

For the DISORT model, we specified the number of streams to be 16, and the Henyey-Greenstein phase function is adopted. Figs. 11 and 12 show the simulated nadir and directional snow emissivity spectra. The shape of snow emissivity, and its radial and angular dependence, is well simulated. The spectral variability of simulated snow emissivity between different view angles is larger than that of measured snow emissivity. The RMSE of simulated nadir and directional snow emissivity spectra lie

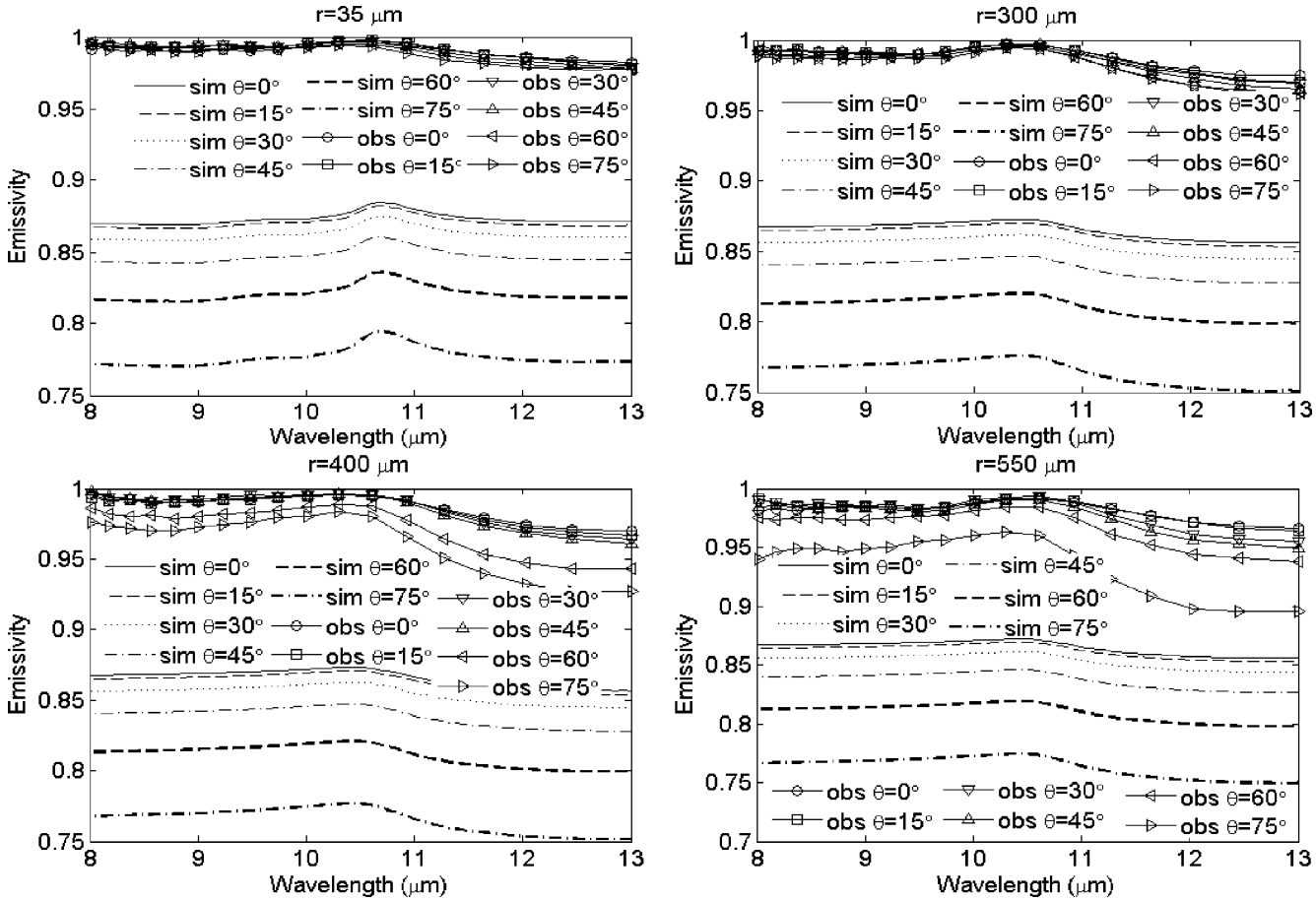


Fig. 10. Comparison of field measured snow directional emissivity spectra with that simulated by the Mie/Hapke model.

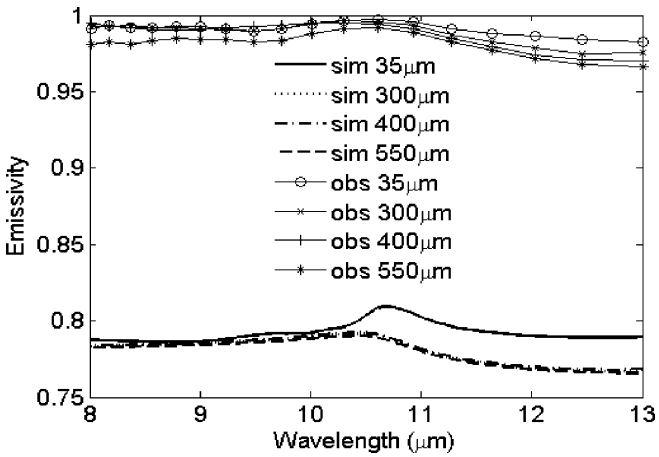


Fig. 11. Comparison of field-measured snow nadir emissivity spectra with that simulated by the Mie/DISORT model.

between 0.042 and 0.209 in the 8-11 $\mu$m and 11-13 $\mu$m spectral regions, as shown in Table V.

### *E. Mie-Corrected/Conel Model*

The simulated snow nadir emissivity spectra are shown in Fig. 13. The shape of snow emissivity is well simulated. The spectral variability of simulated snow emissivity between different radii is very small, while that of measured snow emissivity is relatively large. The RMSE of the Mie-Wald/Conel model are less than 0.005 and 0.004, respectively, in the 8-11 $\mu$m and 11-13 $\mu$m spectral regions. While the RMSE of the Mie-Mishcheko/Conel model is less than 0.012 and 0.020, respectively, in the 8-11 $\mu$m and 11-13 $\mu$m spectral regions (Table II).

### *F. Mie-Corrected/Hapke Model*

The simulated snow nadir emissivity spectra are shown in Fig. 14. The shape of snow emissivity is well simulated. The spectral variability of simulated snow emissivity for different radii is very small, while that of measured snow emissivity is relatively large. As shown in Table II, the RMSE of the Mie-Wald/Hapke model is much lower than that of the Mie-mishcheko/Hapke model. The RMSE of Mie-Wald/Hapke model is less than 0.008 for r = 400, 300, and 550 $\mu$m. In the 8-11 $\mu$m spectral region, the RMSE of the Mie-mishcheko/Hapke model is less than 0.005 for r = 35, 300, and 400 $\mu$m, while the RMSE is 0.012 for r = 550 $\mu$m.

The simulated snow directional emissivity spectra are shown in Fig. 15. The shape of snow emissivity and the angular dependence are well simulated. Compared with measured snow directional emissivity, the spectral variability of snow emissivity simulated with the Mie-Mishchenko/Hapke model between different view angles is very small. The RMSE of simulated directional emissivity is shown in Table VI. The RMSE in the 8-11 $\mu$m spectral region is clearly lower

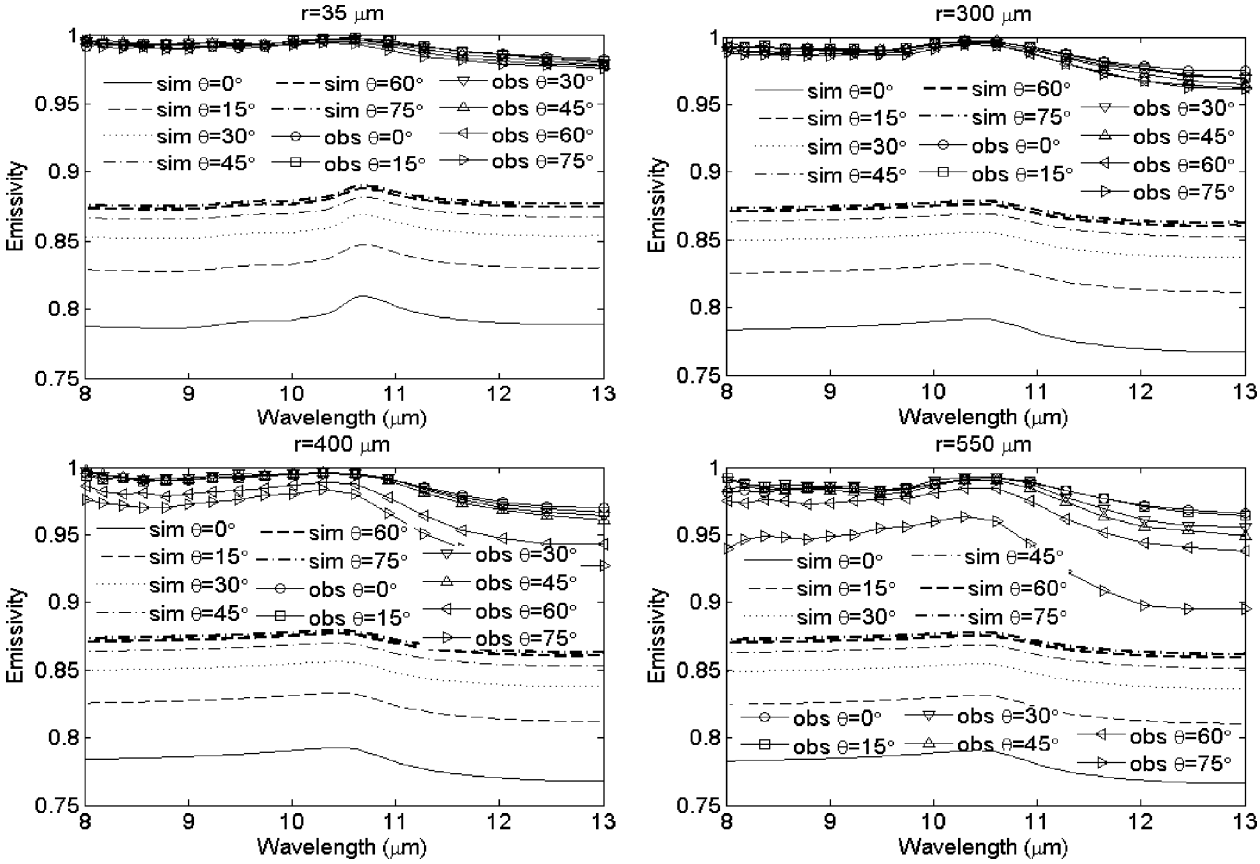


Fig. 12. Comparison of field-measured snow directional emissivity spectra with that simulated by the Mie/DISORT model.

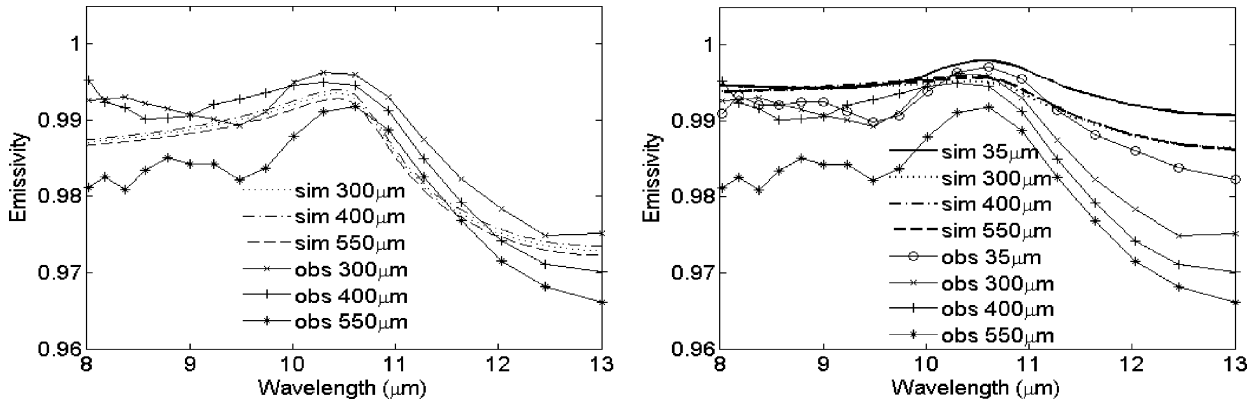


Fig. 13. Comparison of field-measured snow nadir emissivity spectra with that simulated by the Mie-wald/Conel (left) and Mie-mishchenko/Conel models (right, $f = 0.2$).

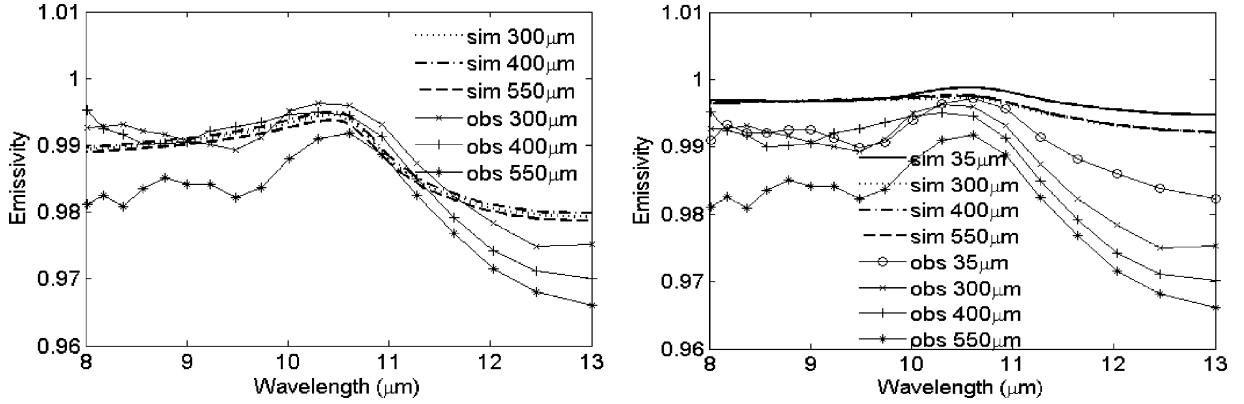


Fig. 14. Comparison of field-measured snow nadir emissivity spectra with that simulated by the Mie-Wald/Hapke (left) and Mie-Mishchenko/Hapke models (right, $f = 0.2$).

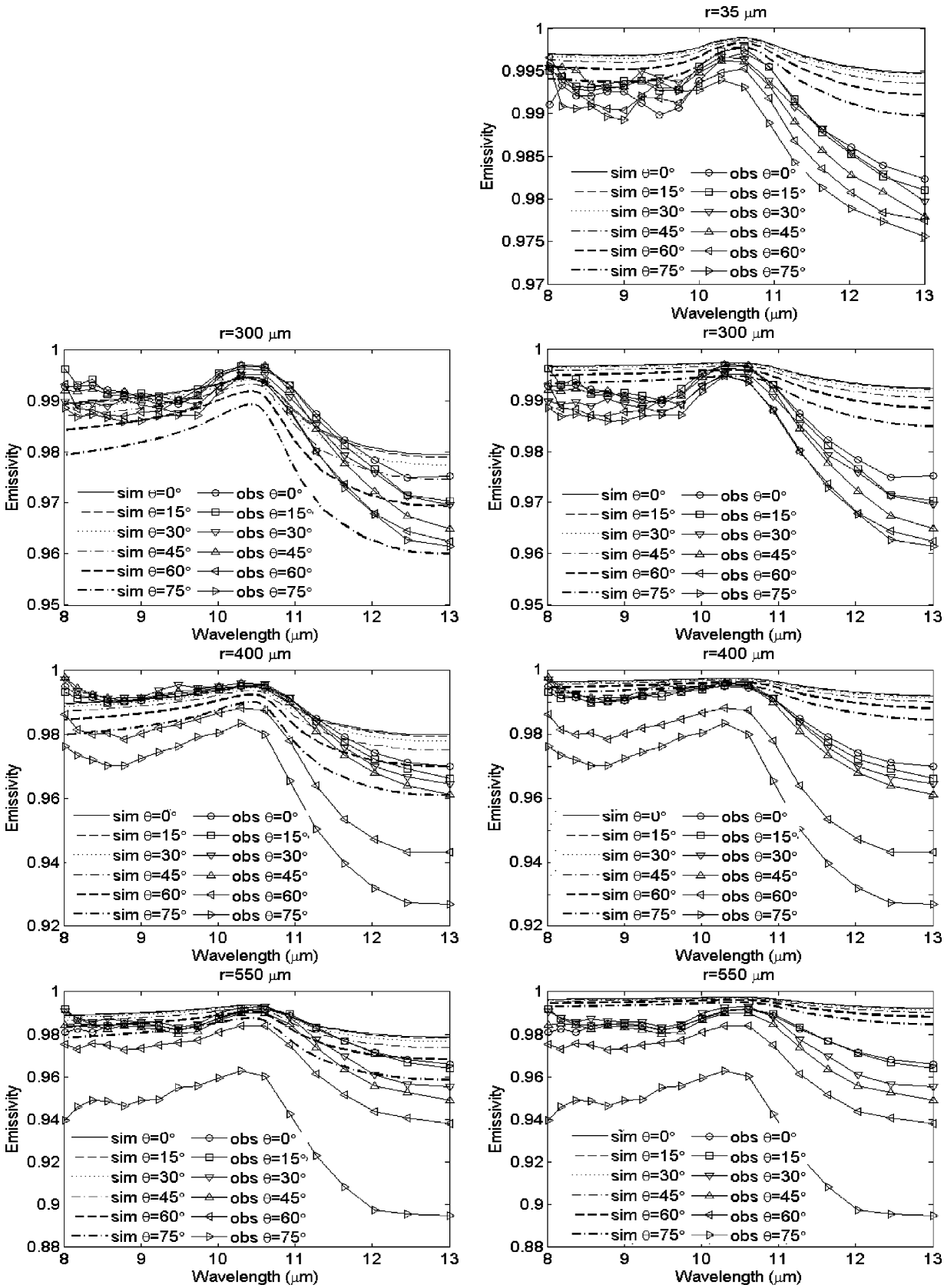


Fig. 15. Comparison of field-measured snow directional emissivity spectra with that simulated by the Mie-Wald/Hapke (left) and the Mie-Mishchenko/Hapke models (right, f = 0.2).

than that in the 11-13 $\mu$m spectral region. The RMSE of the Mie-Mishchenko/Hapke model is less than 0.005 in the 8-11 $\mu$m spectral region for r = 35 $\mu$m; the RMSE of the Mie-Wald/Hapke model is less than 0.006 for r = 300 $\mu$m, while the RMSE of the Mie-Mishchenko/Hapke model is less than 0.007 in the 8-11 $\mu$m spectral region; in the 8-11 $\mu$m

TABLE VI
RMSE OF SIMULATED EMISSIVITIES USING THE MIE-CORRECTED/HAPKE MODEL IN THE8-11 $\mu$m AND11-13 $\mu$m SPECTRAL REGIONS. THE VALUES IN PARENTHESES ARE THE RMSE OF THE MIE-MISHCHENKO/HAPKE MODEL

| Observation angle | RMSE | | | | | | | |
|---|---|---|---|---|---|---|---|---|
| | 8-11 μm | | | | 11-13 μm | | | |
| | Type 1 | Type 2 | Type 3 | Type 4 | Type 1 | Type 2 | Type 3 | Type 4 |
| 0° | -(0.005) | 0.002(0.005) | 0.001(0.005) | 0.006(0.012) | -(0.009) | 0.002(0.014) | 0.007(0.018) | 0.008(0.020) |
| 15° | -(0.003) | 0.003(0.004) | 0.001(0.005) | 0.005(0.011) | -(0.010) | 0.005(0.016) | 0.008(0.019) | 0.009(0.021) |
| 30° | -(0.003) | 0.002(0.007) | 0.003(0.003) | 0.003(0.009) | -(0.010) | 0.005(0.017) | 0.009(0.021) | 0.015(0.029) |
| 45° | -(0.003) | 0.004(0.004) | 0.004(0.003) | 0.005(0.012) | -(0.011) | 0.005(0.018) | 0.009(0.022) | 0.017(0.032) |
| 60° | -(0.004) | 0.003(0.006) | 0.005(0.013) | 0.010(0.019) | -(0.012) | 0.004(0.020) | 0.023(0.040) | 0.024(0.042) |
| 75° | -(0.004) | 0.006(0.006) | 0.009(0.019) | 0.030(0.042) | -(0.012) | 0.006(0.018) | 0.029(0.051) | 0.058(0.083) |

TABLE VII
RMSE OF SIMULATED EMISSIVITY'S USING MIE-CORRECTED/DISORT MODEL IN THE8-11 $\mu$m AND11-13 $\mu$m SPECTRAL REGIONS. THE VALUES IN PARENTHESES ARE THE RMSE OF THE MIE-MISHCHENKO/DISORT MODEL

| Observation angle | RMSE | | | | | | | |
|---|---|---|---|---|---|---|---|---|
| | 8-11 μm | | | | 11-13 μm | | | |
| | Type 1 | Type 2 | Type 3 | Type 4 | Type 1 | Type 2 | Type 3 | Type 4 |
| 0° | -(0.003) | 0.008(0.003) | 0.007(0.002) | 0.003(0.010) | -(0.006) | 0.012(0.009) | 0.008(0.013) | 0.007(0.015) |
| 15° | -(0.002) | 0.005(0.003) | 0.004(0.004) | 0.004(0.010) | -(0.009) | 0.005(0.014) | 0.004(0.017) | 0.004(0.019) |
| 30° | -(0.003) | 0.002(0.006) | 0.004(0.003) | 0.003(0.009) | -(0.010) | 0.004(0.016) | 0.008(0.020) | 0.015(0.028) |
| 45° | -(0.003) | 0.002(0.005) | 0.002(0.004) | 0.007(0.013) | -(0.012) | 0.009(0.020) | 0.012(0.024) | 0.021(0.034) |
| 60° | -(0.005) | 0.003(0.008) | 0.010(0.015) | 0.015(0.021) | -(0.014) | 0.013(0.024) | 0.032(0.043) | 0.034(0.046) |
| 75° | -(0.006) | 0.004(0.009) | 0.018(0.023) | 0.040(0.046) | -(0.016) | 0.014(0.025) | 0.047(0.058) | 0.078(0.089) |

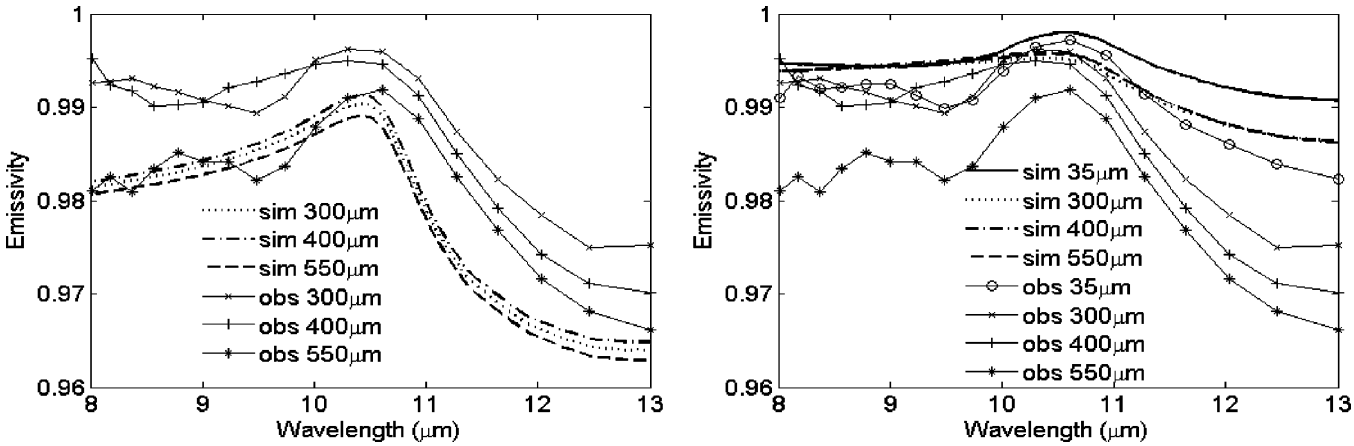


Fig. 16. Comparison of field-measured snow nadir emissivity spectra with that simulated by the Mie-Wald/DISORT (left) and Mie-Mishchenko/DISORT models (right, f = 0.2).

spectral region, the RMSE of the Mie-Wald/Hapke model is less than 0.004 for r = 400 $\mu$m, while the RMSE of the Mie-Mishchenko/Hapke model is less than 0.005 when the view angle is less than 60 degrees; when the view angle is less than 60 degrees, the RMSE of the Mie-Wald/Hapke model is less than 0.006 in the 8-11 $\mu$m spectral region for r = 550 $\mu$m, while the RMSE of the Mie-Mishchenko/Hapke model is less than 0.012 in 8-11 $\mu$m spectral region.

### G. Mie-Corrected/DISORT Model

The simulated snow nadir emissivity spectra are shown in Fig. 16. The shape of snow emissivity is well simulated. The spectral variability of simulated snow emissivity between different radii is very small, while that of measured snow emissivity is relatively large. As shown in Table II, in the 8-11 $\mu$m spectral region the RMSE of the Mie-Wald/DISORT model is less than 0.008 for r = 400, 300, and 550 $\mu$m, while the RMSE of the Mie-Mishcheko/DISORT model is less than 0.010 for r = 35, 400, 300, and 550 $\mu$m; in the 11-13 $\mu$m spectral region, the RMSE of the Mie-Wald/DISORT model is less than 0.012 for r = 400, 300, and 550 $\mu$m, while the RMSE of the Mie-Mishcheko/DISORT model is less than 0.015 for r = 35, 400, 300, and 550 $\mu$m.

The simulated snow directional emissivity spectra are shown in Fig. 17. The shape of snow emissivity and the angular dependence are well simulated. Compared with measured snow directional emissivity, the spectral variability of snow emissivity simulated by the Mie-Mishchenko/DISORT model between different view angles is very small. The RMSE of simulated directional emissivity is shown in Table VII. The RMSE in the 8-11 $\mu$m spectral region is clearly lower than that in the 11-13 $\mu$m spectral region. The RMSE of the Mie-Mishchenko/DISORT model is less than 0.006 for r = 35 $\mu$m in the 8-11 $\mu$m spectral region; the RMSE of the Mie-Wald/DISORT model is less than 0.008 for r = 300 $\mu$m, while the RMSE of the Mie-Mishchenko/DISORT model is

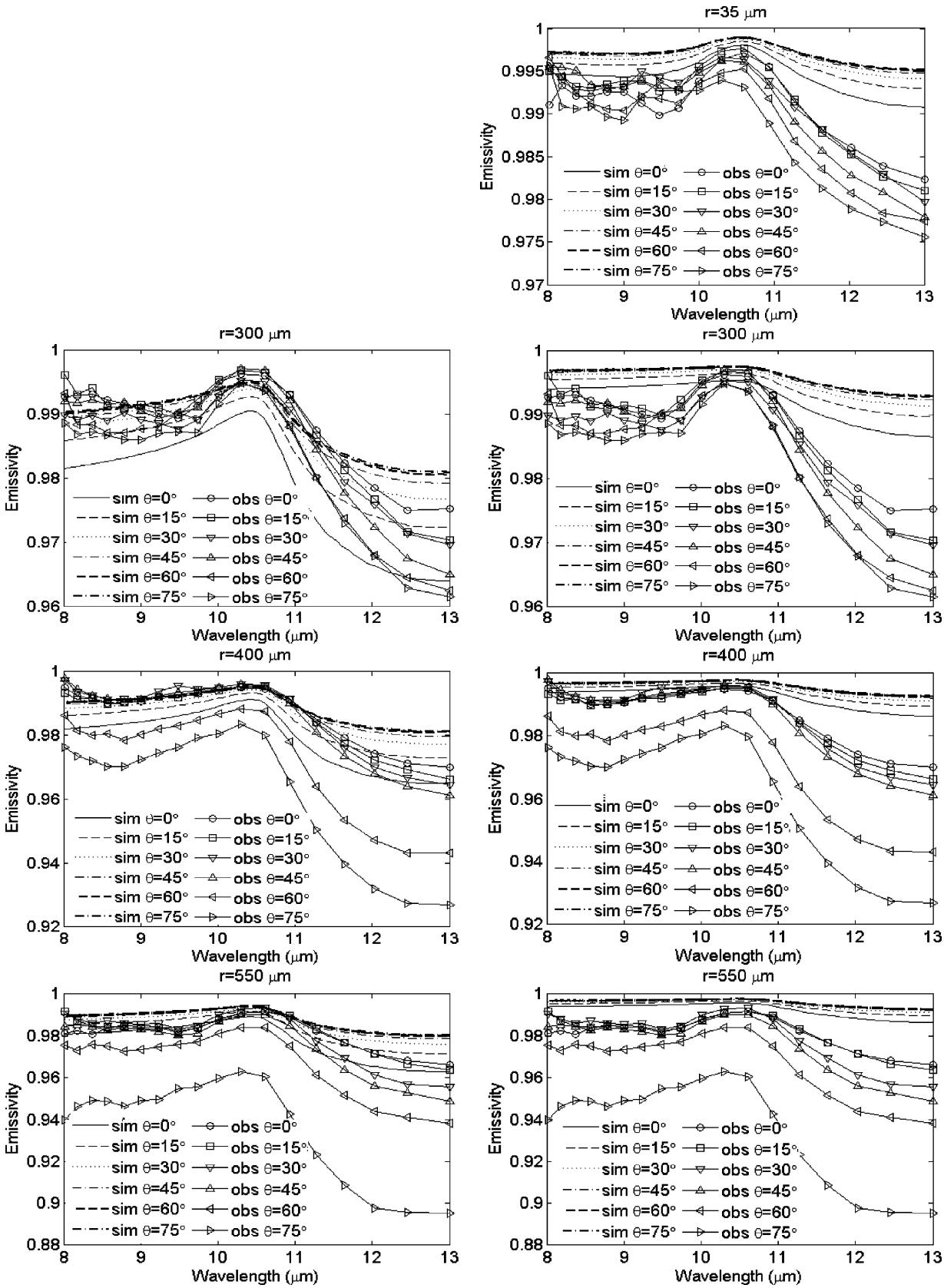


Fig. 17. Comparison of field measured snow directional emissivity spectra with that simulated by the Mie-Wald/DISORT (left) and Mie-Mishchenko/DISORT models (right, $f = 0.2$).

less than 0.009 in the 8-11 $\mu$m spectral region; in 8-11 $\mu$m spectral region, the RMSE of the Mie-Wald/DISORT model is less than 0.007 for $r = 400$ $\mu$m, while the RMSE of the Mie-Mishchenko/DISORT model is less than 0.004, on the condition that the view angle is less than 60 degrees; when the view angle is less than 60 degrees, the RMSE of the

Mie-Wald/DISORT model is about 0.007 for r = 550 $\mu$m, while the RMSE of the Mie-Mishchenko/DISORT model is about 0.013 in the 8-11 $\mu$m spectral region.

## V. Conclusions and Discussions

This paper investigates the applicability of several RT models for snow thermal infrared directional emissivity spectra simulation, and compares each models' simulation results to field-measured snow directional emissivity spectra. In the modeling, the single-scattering albedo and asymmetry factor calculated by the Mie theory, in conjunction with that modified by two existing packing correction methods (i.e., diffraction subtraction and static structure factor correction), are used as inputs to three analytical RT models and one numerical RT model. These models are referred as the Mie/Conel model, Mie/DW model, Mie/Hapke model, Mie/DISORT model, Mie-corrected/Conel model, the Mie-corrected/Hapke model, and the Mie-corrected/DISORT model.

In general, the shape of snow emissivity spectra and its angular dependence are well simulated. The particle radii dependence of snow emissivity spectra is also well simulated, except for the Mie/DW model. The maximum of the simulated emissivity occurs at 10.5 $\mu$m. It is consistent with *in situ* measurements. The consistency between simulated and measured snow emissivity in the 8-11 $\mu$m spectra region is superior to that in the 11-13 $\mu$m spectra region. The modeling ability of the Mie/Conel, Mie/Hapke and Mie/DISORT models is very poor, which implies that the independent scattering assumption does not hold true for a densely packed medium.

For snow nadir emissivity spectra modeling, the Mie-Mishchenko/Conel, Mie-Mishchenko/Hapke and Mie-Mishchenko/DISORT models are appropriate for r = 35 $\mu$m; as their RMSE is less than 0.005 in the 8-11 $\mu$m spectra region. For the other three particles, the Mie-Wald/Conel model is the best choice for snow nadir emissivity modeling; as their RMSE is less than 0.005 in the 8-11 $\mu$m spectra region. For snow directional emissivity modeling, the Mie-corrected/Hapke model is the best choice. The RMSE of the Mie-Mishchenko/Hapke model is less than 0.005 for r = 35 $\mu$m in the 8-11 $\mu$m spectra region; the RMSE of the Mie-Wald/Hapke model is less than 0.006 for $r$ = 300 in the 8-13 $\mu$m spectra region; the RMSE is less than 0.009 for r = 400 $\mu$m in the 8-11 $\mu$m spectra region; and the RMSE is less than 0.006 for r = 550 $\mu$m in the 8-11 $\mu$m spectra region, except for 60 and 75 degree view angles.

As pointed out by Hapke [36], the diffraction contribution to the scattering cross section and volume single-scattering phase function must be removed in a densely packed medium. Diffraction subtraction and static structure factor are used to modify the Mie parameters in this study, and their role in improving the modeling is pronounced. The simulation results in 11-13 $\mu$m are barely satisfactory, and the error is very significant, especially for large view angles. However, the accuracy of field-measured snow emissivity is on the order of 0.01 [28]. Furthermore, there is still no effective method for calculating single-scattering parameters for densely packed particulates. Other complicated physical processes, such as shadow hiding and coherent backscattering, are not included in the packing correction method [25], [37], [38]. Surface roughness should be considered if these RT models are used to simulate snow surface emissivity at the remote sensing pixel scale, or at the scale of climate models.

## Acknowledgment

The authors would like to express their sincere gratitude to Prof. Hori for providing *in situ* measurements. They would also like to thank the reviewer for the valuable comments and suggestions that improved the presentation of this paper.

## References

[1] J. Key and M. haefliger, "Arctic ice surface temperature retrieval from AVHRR thermal channels," *J. Geophys. Res.*, vol. 97, pp. 5885–5893, 1992.

[2] Z. Wan and J. Dozier, "A generalized split-window algorithm for retrieving land-surface temperature form space," *IEEE Trans. Geosci. Remote Sens.*, vol. 34, pp. 892–905, 1996.

[3] Y. Plokhenko and W. P. Menzel, "The effects of surface reflection on estimating the vertical temperature-humidity distribution from spectral infrared measurements," *J. Appl. Meteorol.*, vol. 39, pp. 3–12, 2000.

[4] R. Beer, T. A. Glavich, and D. M. Rider, "Tropospheric emission spectrometer for the earth observing system's aura satellite," *Appl. Opt.*, vol. 40, pp. 2356–2367, 2001.

[5] C. Clerbaux, J. Hadji-Lazaro, S. Payan, C. Camy-Peyret, C. Wang, and D. P. Edwards, "Retrieval of CO from nadir remote-sensing measurements in the infrared using four different inversion algorithms," *Appl. Opt.*, vol. 41, pp. 7068–7078, 2002.

[6] N. Bormann, P. Bauer, G. Kelly, M. Matricardi, and J. N. Thepaut, "Status and plans for the assimilation of infrared and microwave radiances over land at ECWMF," in *1st Workshop on Remote Sensing and Modeling of Surface Parameters*, Paris, France, 2006.

[7] G. B. Bonan, K. W. Oleson, M. Vertenstein, S. Levis, X. Zeng, Y. Dai, R. E. Dickinson, and Z.-L. Yang, "The land surface climatology of the community land model coupled to the NCAR community climate model," *J. Climate*, vol. 15, pp. 3123–3149, 2002.

[8] G. Mie, "Beitrage zur optik truber medien speziell kolloidaler metrllosungen (Contribution to the optics of turbid media, particulary of colloidal metal solutions)," *Ann. Phys.*, vol. 25, pp. 377–445, 1908.

[9] J. E. Conel, "Infrared emissivities of silicates: Experimental results and a cloudy atmosphere model of spectral emission from condensed particulate mediums," *J. Geophys. Res.*, vol. 74, pp. 1614–1634, 1969.

[10] W. J. Wiscombe and S. G. Warren, "A model for the spectral albedo of snow. I. Pure snow," *J. Atmospher. Sci.*, vol. 37, pp. 2712–2733, 1980.

[11] J. Dozier and S. G. Warren, "Effect of viewing angle on the thermal infrared brightness temperature of snow," *Water Resource Res.*, vol. 18, pp. 1424–1434, 1982.

[12] J. H. Joseph, W. J. Wiscombe, and J. A. Weinman, "The delta-Eddington approximation for radiative flux transfer," *J. Atmospher. Sci.*, vol. 33, pp. 2452–2459, 1976.

[13] B. Hapke, "Bidirectional reflectance spectroscopy. 1. Theory," *J. Geophys. Res.*, vol. 86, pp. 3039–3054, 1981.

[14] B. Hapke, "Birdirectional reflectance spectroscopy. 3. Correction for macroscopic roughness," *Icarus*, vol. 59, pp. 41–59, 1984.

[15] B. Hapke, "Bidirectional reflectance spectroscopy. 4. The extinction coefficient and the opposition effect," *Icarus*, vol. 67, pp. 264–280, 1986.

[16] B. Hapke, *Theory of Reflectance and Emittance Spectroscopy*. New York, NY: Cambridge Univ. Press, 1993.

[17] S. Liang, *Quantitative Remote Sensing of Land Surface*. New York, NY: Wiley, 2004, p. 534.

[18] S. Liang and J. R. G. Townshen, "A modified Hapke model for soil bidirectional reflectance," *Remote Sens. Environ.*, vol. 55, pp. 1–10, 1996.

[19] K. Stamnes, S.-C. Tsay, W. J. Wiscombe, and K. Jayaweera, "Numerically stable algorithm for discrete-ordinate-method radiative transfer in multiple scattering and emitting layered media," *Appl. Opt.*, vol. 27, pp. 2502–2509, 1988.

[20] K. Stamnes, W. Li, H. Eide, T. Aoki, M. Hori, and R. Storvold, "ADEOS-II/GLI snow/ice products. Part I: Scientific basis," *Remote Sens. Environ.*, vol. 111, pp. 258–273, 2007.

[21] V. d. Hulst, *Light Scattering by Small Particles*. New York, NY: Dover, 1957.

[22] A. E. Wald, "Modelling thermal infrared (2–14 $\mu$m) reflectance spectra of frost and snow," *J. Geophys. Res.*, vol. 99, 1994.

[23] A. E. Wald and J. W. Salisbury, "Thermal infrared directional emissivity of powered quartz," *J. Geophys. Res.*, vol. 100, 1995.
[24] M. I. Mishchenko and A. Macke, "Asymmetry parameters for the phase function for isolated and densely packed spherical particles with multiple internal inclusions on the geometric optics limit," *J. Quantitative Spectrosc. Radiative Transfer*, vol. 57, pp. 767–794, 1997.
[25] M. I. Mishchenko, "Asymmetry parameters of the phase function for densely packed scattering grains," *J. Quantitative Spectrosc. Radiative Transfer*, vol. 52, pp. 95–110, 1994.
[26] S. G. Warren and R. E. Brandt, "Optical constants of ice from the ultraviolet to the microwave: A revised compilation," *J. Geophys. Res.*, vol. 113, 2008, DOI: 10.1029/2007JD009744.
[27] S. G. Warren, "Optical constants of ice from the ultraviolet to the microwave," *Appl. Opt.*, vol. 23, pp. 1206–1225, 1984.
[28] M. Hori, T. Aoki, T. Tanikawa, H. Motoyoshi, A. Hachikubo, K. Sugiura, T. J. Yasunari, H. Eide, R. Storvold, Y. Nakajima, and F. Takahashi, "In-situ measured spectral directional emissivity of snow and ice in the 8–14 $\mu$m atmospheric window," *Remote Sens. Environ.*, vol. 100, pp. 486–502, 2006.
[29] W. Wiscombe, "Improved Mie scattering algorithm," *Appl. Opt.*, vol. 19, pp. 1505–1509, 1980.
[30] A. W. Nolin and S. Liang, "Progress in bidirectional reflectance modeling and applications for surface particulate media: Snow and soils," *Remote Sens. Rev.*, vol. 18, pp. 307–342, 2000.
[31] A. W. Nolin and J. Dozier, "A hyperspectral method for remotely sensing the grain size of snow," *Remote Sens. Environ.*, vol. 74, 2000.
[32] T. H. Painter and J. Dozier, "Measurements of the hemispherical-directional reflectance of snow at fine spectral and angular resolution," *J. Geophys. Res.*, vol. 109, 2004, DOI: 10.1029/2003JD004458.
[33] S. Li and X. Zhou, "Modelling and measuring the spectral bidirectional reflectance factor of snow-covered sea ice: An intercomparison study," *Hydrological Processes*, vol. 18, pp. 3559–3581, 2004.
[34] M. I. Mishchenko, J. M. Dlugach, E. G. Yanovitskij, and N. T. Zakharova, "Bidirectional reflectance of flat optically thick particulate layers-an efficient radiative transfer solution and applications to snow and soil surfaces," *J. Quantitative Spectrosc. Radiative Transfer*, vol. 63, pp. 409–432, 1999.
[35] M. I. Mishchenko, L. D. Travis, and A. A. Lacis, *Scattering, Absorption, and Emission of Light by Small Particles*. Cambridge, U.K.: Cambridge Univ. Press, 2002.
[36] B. Hapke, "Scattering and diffraction of light by particles in planetary regoliths," *J. Quantitative Spectrosc. Radiative Transfer*, vol. 61, pp. 565–581, 1999.
[37] B. Hapke, "Bidirectional reflectance spectroscopy. 5. The coherent backscattering opposition effect and anisotropic scattering," *Icarus*, vol. 157, pp. 523–524, 2002.
[38] S. Liang and M. I. Mishchenko, "Calculations of the soil hot-spot effect using the coherent backscattering theory," *Remote Sens. Environ.*, vol. 60, pp. 163–173, 1997.

**Jie Cheng** received the B.Sc. degree in survey and mapping from East China Institute of Technology, Fuzhou, China, in 2002, and the Ph.D. degree in cartography and remote sensing from the Institute of Remote Sensing Applications of Chinese Academy of Sciences, Beijing, China, in 2008.

He was a Postdocotral Fellow in the State Key Laboratory of Remote Sensing Science, Beijing Normal University, from 2008 to 2010 and an Assistant Research Scientist at the University of Maryland, College Park, from 2009 to 2010. He is currently an Assistant Professor in the College of Global Change and Earth System Sciences, Beijing Normal University. His main research interests focus on surface temperature and emissivity retrieval from hyperspectral data, surface emissivity modeling and trace gases inversion using remotely sensed data.

**Shunlin Liang** (M'94–SM'01) received the Ph.D. degree in remote sensing and GIS from Boston University, Boston, MA.

He was a Postdoctoral Research Associate with Boston University from 1992 to 1993 and a Validation Scientist with the NOAA/NASA Pathfinder AVHRR Land Project from 1993 to 1994. He is currently a Professor with the University of Maryland, College Park. His main research interests focus on spatio-temporal analysis of remotely sensed data, integration of data from different sources and numerical models, and linkage of remote sensing with global environmental changes. He authored the book *Quantitative Remote Sensing of Land Surfaces* (Wiley, 2004) and edited the book *Advances in Land Remote Sensing: System, Modeling, Inversion and Application* (Springer, 2008).

Dr. Liang is a member of NASA ASTER and MODIS science teams and NOAA GOES-R Land science team. He is a co-chairman of the International Society for Photogrammetry and Remote Sensing Commission VII/I Working Group on Fundamental Physics and Modeling. He is an Associate Editor of the IEEE TRANSACTIONS ON GEOSCIENCE AND REMOTE SENSING and also a guest editor of several remote sensing journals.

**Fuzhong Weng** received the M.S. degree in radar meteorology from the Nanjing Institute of Meteorology, Nanjing, China, in 1985 and the Ph.D. degree from Colorado State University, Fort Collins, in 1992.

He is currently the Chief of the Sensor Physics Branch of the NOAA/NESDIS Center for Satellite Applications and Research, Camp Springs, MD. He has been leading the developments of NOAA operational satellite microwave products and algorithms from the Special Sensor Microwave/Image and Advanced Microwave Sounding Unit. He is a NPOESS microwave operational algorithm team member. He is a Science Lead in developing the community radiative transfer model (CRTM) that has been successfully used in several operational data assimilation systems in the U.S. He also directly contributed to the developments of microwave land, snow, and sea-ice emissivity models, which have significantly improved uses of satellite sounding data in NWP models and impacted high-latitude weather forecasts. He is currently developing new innovative techniques to advance the uses of satellite measurements under cloudy and precipitation areas in NWP models. He has published over 70 papers in international peer-reviewed journals.

Dr. Weng was the first winner of the 2000 NOAA David Johnson Award for his outstanding contributions to satellite microwave remote sensing fields and the utilization of satellite data in NWP models. He also received the 2002 SPIE Scientific Achievement Award for Excellence in Developing Operational Satellite Microwave Products and Algorithms. He was awarded in 2004 by U.S. Department of commerce with a Bronze Medal for his developments of operational microwave products to improve weather and climate predictions. He is the winner of U.S. Department of Commerce Gold Medal Award in 2005 for his achievement in satellite data assimilation, and he also received the NOAA bronze medal for leading successful NOAA-18 instrument calibration.

**Jindi Wang** graduated from the Beijing University of Posts and Telecommunications, Beijing, China, in 1982.

She is currently a Professor at State Key Laboratory of Remote Sensing Science, Research Center for Remote Sensing and GIS, Beijing Normal University, Beijing, China. Her primary research interests focus on land surface BRDF modeling, land surface parameters retrieval from various remotely sensed data, typical land surface objects' spectrum library building and its applications.

**Xiaowen Li** graduated from the Chengdu Institute of Radio Engineering, China, in 1968. He received the M.A. degree in geography and the M.S. degree in electric and computer engineering and the Ph.D. degree in geography from the University of California, Santa Barbara, in 1981 and 1985, respectively.

He is with the State Key Laboratory of Remote Sensing Science, Research Center for Remote Sensing and GIS, Beijing Normal University, China, and also with the Institute of Remote Sensing Applications of Chinese Academy of Sciences, China. Before this, he was a Research Professor at the Center for Remote Sensing, Department of Geography, Boston University, Boston, MA. He established the vegetation bidirection reflection Li-Strahler geometric optics model. He initiated the ill-conditioned inversion theory in the field of quantitative remote sensing. On the study of the applicability of the Helmholz reciprocity principle in the area of ground surface remote sensing, he put forward the limitation conditions of Helmholz reciprocity principle for the nonuniform image element bidirection reflection. With respect to the scale effect of Planck's law in ground surface remote sensing, he set up the conceptual model suitable for non-isothermal surface heat-radiation direction and initiated the scale modifier formula of Planck's law for non-isothermal blackbody plane.